Phase Diagram and Effective Shape of Semiflexible Colloidal Rods and Biopolymers

M. Dennison,[1] M. Dijkstra,[1] and R. van Roij[2]

[1]Soft Condensed Matter, Debye Institute for Nanomaterials Science, Utrecht University, Princetonplein 5, 3584 CC Utrecht, The Netherlands

[2]Institute for Theoretical Physics, Utrecht University, Leuvenlaan 4, 3584 CE Utrecht, The Netherlands

(Received 27 December 2010; revised manuscript received 7 April 2011; published 20 May 2011)

We study suspensions of semiflexible colloidal rods and biopolymers using an Onsager-type second-virial functional for a segmented-chain model. For mixtures of thin and thick fd virus particles, we calculate full phase diagrams, finding quantitative agreement with experimental observations. We show that flexibility, which renders the rods effectively shorter and thicker depending on the state point, is crucial to understanding the topologies of the phase diagrams. We also calculate the stretching of wormlike micelles in a host fd virus suspension, finding agreement with experiments.

DOI: 10.1103/PhysRevLett.106.208302 PACS numbers: 82.70.Dd, 61.30.Cz, 64.70.M−, 82.35.Pq

Rodlike particles are capable of forming a great variety of liquid-crystalline phases [1], and have been widely explored experimentally and theoretically [2]. Today, a prominent role is being played by aqueous suspensions of fd virus particles, which are charged, semiflexible, Brownian needles with a length-to-diameter ratio exceeding 100, exhibiting isotropic (I), cholesteric nematic (N), smectic, columnar, and crystalline phases upon increasing the concentration [3–5]. Moreover, wild-type fd virus particles have been bioengineered to have, for instance, a polyethylene-glycol (PEG) coating, such that mixtures of thin and thick rods with diameter ratios d varying from 1.1 to 3.7 could be studied experimentally [6]. The resulting phase diagrams are extremely rich, even in the regime where only I and N phases are relevant. The observations not only include I-N coexistence with strong fractionation effects, but also, for $d \gtrsim 3$, two-phase N-N and three-phase I-N-N coexistence with phase diagram topologies that strongly depend on d. Given the needlelike shape of the fd virus particles, and the relative structural simplicity of I and N phases, one would expect these phase diagrams to be well understood, e.g., resembling those of theoretical predictions based on Onsager's second-virial theory for thin-thick mixtures of rigid rods [7]. However, these systems turn out to be surprisingly poorly understood. For instance, the experiments show N-N demixing with a low-density (lower) critical point that shifts to lower densities with increasing d [6], while the theory predicts the exact opposite: a high-density (upper) N-N critical point and N-N demixing that extends to higher densities with increasing d [7,8]. Moreover, the experiments show N-N demixing at diameter ratios as low as $d \gtrsim 2$–3 while rigid-rod models predict $d \gtrsim 4$–5 [6,7]. In this Letter we will show that the key to a real understanding of these systems is flexibility, which renders the needles effectively shorter and fatter depending on the state point [9,10]. In addition, our model and theory can also quantify the observed stretching of guest biopolymers in host suspensions of fd virus particles [11].

One-component systems of semiflexible rods have been studied using numerous methods, and it is known that only a slight flexibility is enough to shift the I-N transition to significantly higher concentrations [12–16]. We follow the segmented-chain model introduced by Wessels and Mulder [16], in which (i) flexibility is incorporated by introducing a bending potential between the chain segments and (ii) excluded volume is taken into account at the segment level. This approach reproduces (in the appropriate limits) the results of Ref. [12], with the advantage of only having to deal with a discrete number of degrees of freedom. Here, we generalize this model to two-component systems and map out, for the first time, the full phase behavior beyond stability analysis. Moreover, we calculate the effective particle shape, which turns out to be strongly state-point dependent.

We consider a suspension of N_i semiflexible rods of species $i = 1, 2$ with contour lengths L_i, in a volume V at temperature T. Following Ref. [16] we model a rod of species i as a chain of M_i rodlike segments of length $l_i = L_i/M_i$ and diameter $D_i \ll l_i$. Denoting the orientation of the mth segment by a unit vector ω_m (with $1 \le m \le M_i$), we write the bending energy of a chain of species i with orientation $\mathbf{\Omega} = \{\omega_1, \ldots, \omega_{M_i}\}$ as

$$U_i(\mathbf{\Omega}) = \sum_{m=1}^{M_i-1} u_i(\omega_m, \omega_{m+1}) = -\frac{P_i}{l_i} \sum_{m=1}^{M_i-1} \omega_m \cdot \omega_{m+1}, \quad (1)$$

where stiffness is described in terms of the persistence length P_i [16]. Throughout we use thermal energy units by setting $k_B T = 1$. The state of the suspension is characterized by the orientation distribution functions (ODFs) $f_i(\mathbf{\Omega})$, which satisfy the normalization condition $\int d\mathbf{\Omega} f_i(\mathbf{\Omega}) = 1$, where $d\mathbf{\Omega} = \prod_{m=1}^{M_i} d\omega_m$. Denoting the total number of rods by $N = N_1 + N_2$, the density by $\rho = N/V$, and the mole fraction of species i by $x_i = N_i/N$, we generalize the variational free energy functional in Ref. [16] to $F[f_1, f_2]$ to describe binary mixtures within an Onsager-like second-virial approximation as

$$\frac{F[f_1,f_2]}{N} = \ln(B\rho) - 1 + x_1 \ln x_1 + x_2 \ln x_2 + \sum_{i=1}^{2} x_i \int f_i(\mathbf{\Omega})\{\ln[4\pi f_i(\mathbf{\Omega})] + U_i(\mathbf{\Omega})\} d\mathbf{\Omega} + \frac{\rho}{2} \sum_{i,j=1}^{2} x_i x_j \int f_i(\mathbf{\Omega}) f_j(\mathbf{\Omega}') K_{ij}(\mathbf{\Omega}, \mathbf{\Omega}') d\mathbf{\Omega} d\mathbf{\Omega}'. \quad (2)$$

The first line of Eq. (2) represents the translational and the mixing ideal-gas contributions (with $B = \frac{\pi}{4} D_1 L_1^2$, a constant), the second line denotes the orientation entropy and bending energy, and the third line the excluded volume interactions, which can be considered at the segment level with $K_{ij}(\mathbf{\Omega}, \mathbf{\Omega}') = \sum_{m=1}^{M_i} \sum_{m'=1}^{M_j} k_{ij}(\omega_m, \omega_{m'})$. For $M_i = 1$ and $U_i \equiv 0$, Eq. (2) reduces to the Onsager functional for binary mixtures of rigid rods [7,17]. From hereon, we simply summarize our method and direct those interested in the complete outline to Ref. [8]. At a given thermodynamic state point, the equilibrium ODFs minimize F and therefore satisfy

$$f_i(\mathbf{\Omega}) = \frac{\exp[-U_i(\mathbf{\Omega}) - V_i(\mathbf{\Omega})]}{Q_i}, \quad (3)$$

$$V_i(\mathbf{\Omega}) = \rho \sum_{j=1}^{2} x_j \int K_{ij}(\mathbf{\Omega}, \mathbf{\Omega}') f_j(\mathbf{\Omega}') d\mathbf{\Omega}', \quad (4)$$

where $V_i(\mathbf{\Omega})$ can be seen as a self-consistent field acting on all segments of a chain, and Q_i is a partition functionlike normalization factor [16]. Explicitly solving Eqs. (3) and (4) for state points of interest would be prohibitively expensive computationally due to the high-dimensional angular $\mathbf{\Omega}$ grids that would be required in the case when $M_i \gg 1$. Instead, we formally evaluate the functional F of Eq. (2) in its minimum by inserting the solutions f_i of Eqs. (3) and (4) to find the equilibrium free energy

$$\frac{F_{\mathrm{eq}}}{N} = \ln(B\rho) - 1 + x_1 \ln\frac{x_1}{Q_1} + x_2 \ln\frac{x_2}{Q_2} - \frac{1}{2}\rho \times \sum_{i,j}^{2} x_i x_j \sum_{m=1}^{M_i} \sum_{m'=1}^{M_j} \int k_{ij}(\omega, \omega') f_{i,m}(\omega) f_{j,m'}(\omega') d\omega d\omega', \quad (5)$$

where $f_{i,m}(\omega)$ is the ODF of the mth segment of a chain of species i given by $f_{i,m}(\omega) = \int f_i(\mathbf{\Omega}) \delta(\omega - \omega_m) d\mathbf{\Omega}$. Equation (5) implies that the thermodynamics does not require the full solutions $f_i(\mathbf{\Omega})$ but only the M_i single-segment ODFs $f_{i,m}(\omega)$ and the normalization factors Q_i. The calculation of these is given in Ref. [8]. With the ODFs, and hence F_{eq}, known, all thermodynamic properties such as osmotic pressure Π and phase diagrams follow [7].

We have calculated the phase diagrams for mixtures of bare fd particles (species 1, thin) and PEG-coated ones (species 2, thick), with equal contour and persistence lengths, $L_1 = L_2 = 0.88\ \mu$m and $P_1 = P_2 = 2.2\ \mu$m [6]. The bare fd diameter is fixed to $D_1 = 6.6$ nm, and following the experiments of Ref. [6] we consider several diameter ratios $d = D_2/D_1$ to describe varying thicknesses of the PEG coating. We use sufficient segments per virus particle such that we are in the continuum limit for all state points of interest [8]. In Fig. 1 we show, for several d, the resulting phase diagrams in the (ρ_1, ρ_2) representation, including the scaled [8] experimental data from Ref. [6]. For all d we find isotropic-nematic (I-N) coexistence, with the tie-lines indicating, for increasing d, an increasing fractionation of the thinner and thicker rods preferentially into the I and N phase, respectively.

In agreement with the experiments of Ref. [6], we find no N-N coexistence in the density regime of interest for the smallest diameter ratio $d = 1.2$ [Fig. 1(a)]. For increasing d an N-N demixing regime appears in the density regime of interest, with a lower critical point as shown for $d = 3.1$ in Fig. 1(b); in the experiments of Ref. [6] such a phase diagram was found for $d \simeq 2.9$. Slightly increasing the PEG layer thickness to $d = 3.11$ reveals an I-N-N triple

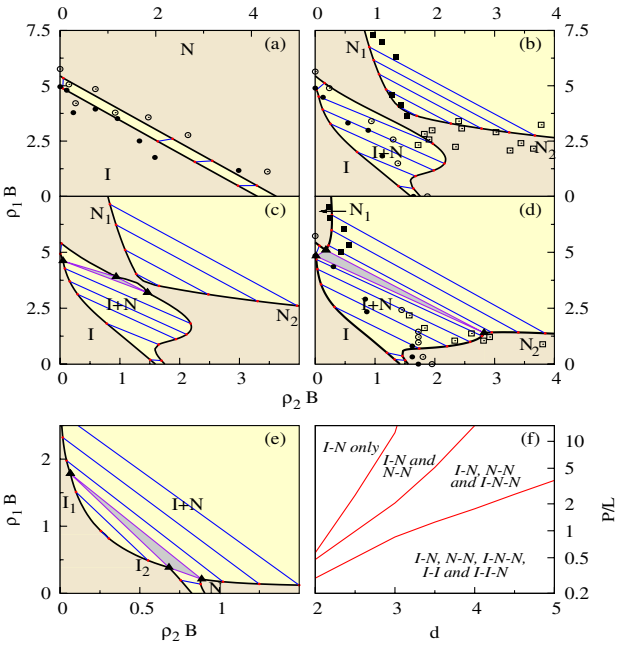

FIG. 1 (color online). Phase diagrams (see text) for mixtures of bare (thin) fd virus particles (species 1) and PEG-coated (thick) ones (species 2), with diameter ratios (a) $d = 1.2$, (b) 3.1, (c) 3.11, (d) 3.5, (e) 6. The lighter colored areas indicate the two-phase regions with tie-lines connecting coexisting state points; triangles denote I-N-N and I-I-N triple points. Experimental results from Ref. [6] are shown by circles (I-N) and squares (N-N) for (a) $d = 1.1$, (b) 2.9, and (d) 3. (f) Topology of the phase diagram (two- and three-phase coexistence) of binary mixtures of (modified) fd virus particles as a function of their diameter ratio d and persistence length P.

point and an associated N-N demixing regime with an upper critical point emerging out of the I-N coexistence regime [Fig. 1(c)]. This N-N upper critical point has not been reported experimentally, perhaps because it only exists in a small regime of diameter ratios: for $d = 3.125$ the upper and lower N-N points have merged to form a single neck-shaped N-N regime that is separated from the I-N coexistence regime by an I-N-N triple point, with the I and one N phase rich in bare fd particles and the other N phase rich in PEG-coated fd particles [Fig. 1(d) shows an example of this behavior for $d = 3.5$]. Interestingly, such neck-shaped phase diagrams have also been reported in Ref. [6] for diameter ratios $d \gtrsim 3$. For $d = 6$, Fig. 1(e) shows an I-I-N triple point and I-I coexistence, as found also for thin-thick mixtures of rigid rods with diameter ratios exceeding $d \simeq 8$ [7]. We find that this behavior is present for $d \gtrsim 4.5$. We also compare our results in Fig. 1 to experimental data from Ref. [6], using a d value that gives the best fit. At low d we find excellent agreement, although we must use a d value of 1.2 (compared to the experimental value of 1.1). For larger d, we tend to slightly overestimate the size of the I-N coexistence region. However, our results are quantitatively much closer to the experimental data than those obtained for rigid rods (see also Ref. [8]).

Motivated by recent progress in the bioengineering of fd virus particles [18], which may allow for tuning their flexibility, we have also calculated phase diagrams for a large variety of diameter ratios and persistence lengths $P_1 = P_2 \equiv P$. Figure 1(f) summarizes our findings by dividing the (d, P) plane into regimes with phase diagrams featuring only an I-N transition (for stiff rods and small d) all the way to complex phase diagrams with I-N, I-I, N-N phase coexistence and I-I-N and I-N-N triple points (for flexible rods and large d). Clearly, increasing d and decreasing P have similar effects on the phase diagram, and hence increasing the flexibility is expected to considerably enhance the complexity of the phase diagrams.

In order for a model system of rigid rods to begin to capture the phase behavior of binary fd virus systems, one must use a system of much shorter, thicker rods, with $L/D \lesssim 7$ for the PEG-coated fd virus [6], much lower than the true values of 20–110. The inference is that long semiflexible rods exhibit the same phase behavior as short rigid rods [9,10]. Our model enables us to define an effective shape, whereby we map the excluded volume of the semiflexible rods onto that of rigid rods. We define the mean square effective length $L_{e,i}^2$ as

$$L_{e,i}^2 = l_i^2 \sum_{m=1}^{M_i} \sum_{m'=1}^{M_i} \int (\omega \cdot \omega') f_{i,m,m'}(\omega, \omega') d\omega d\omega', \quad (6)$$

where $f_{i,m,m'}(\omega, \omega')$ is the pair orientation distribution function (PDF) (calculated in Ref. [8]). We use the PDFs to calculate $L_{e,i}$ and, from this, the effective diameter $D_{e,i}$ required for rigid rods of length $L_{e,i}$ to have the same excluded volume as flexible rods of length L_i.

Figure 2(a) shows the effective shape $L_{e,i}/D_{e,i}$ for a mixture of thick-thin fd virus particles with $d = 3$, throughout the phase diagram [the route we follow is shown in Fig. 2(b), where we use the x_2-Π representation for clarity]. It is immediately apparent that throughout the phase diagram, while the rods always behave as shorter, thicker rods, the effective shape varies considerably. In the isotropic phase, we find for both species $L_{e,i}/D_{e,i}$ to be about 20% of L_i/D_i. This corresponds to $L_e/D_e \approx 8.5$ for the thick rods, close to the $L/D \lesssim 7$ required for rigid-rod systems to capture the phase behavior of these binary systems [6]. For the nematic phase, however, $L_{e,i}/D_{e,i}$ jumps to over 50% of L_i/D_i, and increases considerably as Π is increased. Interestingly, the thick rods stretch out more than the thin rods, with the rods now effectively differing in both diameter and length. We conclude that a fixed effective shape does not capture the essential physics of these suspensions; the state-point dependent stretching of the flexible rods is a key feature.

Finally, we present results for the effective length of semiflexible polymers dissolved in an fd virus suspension. A range of polymers which undergo a coil-rod transition, stretching out over the I-N transition of the host fd virus, has been studied experimentally [11]. Here, we examine wormlike micelles, which have constant $P = 0.5$ μm, $D = 14$ nm and variable $L = 5$–50 μm. The concentration of the polymers is sufficiently low that they can be treated as a single particle in a bulk fd virus suspension, and we study the behavior of the polymer L_e over the I-N phase transition of the fd virus (found at $\Pi B = 29.54$). The results are shown in Fig. 3(a). For the shortest polymers studied, we see a considerable jump in L_e, from $L_e \simeq 0.26L$ to $\simeq 0.61L$, corresponding to a coil-rod transition. For longer polymers, the jump in L_e becomes smaller, and the longest ones only become truly rodlike well into the nematic phase of the fd virus. It is interesting to note that in the isotropic phase, for all cases, L_e appears to remain essentially constant.

In the isotropic fd virus phase, the polymer may be considered along the lines of the Kratky-Porod wormlike chain model [19], generalized to account for excluded

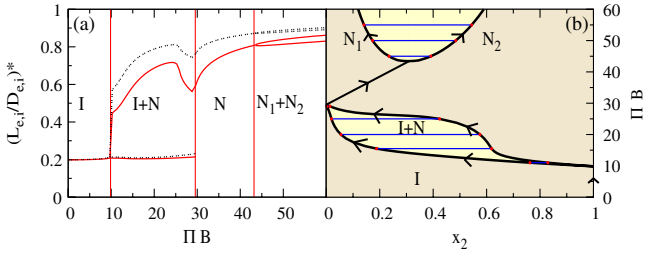

FIG. 2 (color online). (a) Relative effective shape of fd virus particles $(L_{e,i}/D_{e,i})^* = (L_{e,i}/D_{e,i})/(L_i/D_i)$ as a function of osmotic pressure (Π) (solid lines show bare fd, dashed lines show PEG-coated fd), and (b) the path we follow throughout the phase diagram in the x_2-Π representation, indicated by the arrows.

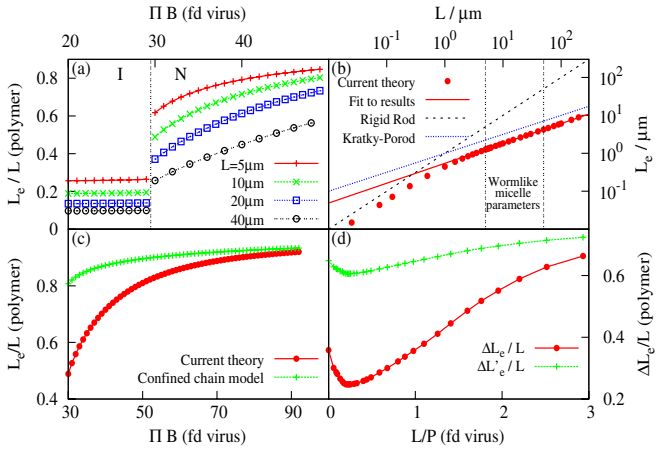

FIG. 3 (color online). (a) L_e of wormlike micelles of various L against host fd virus osmotic pressure Π. (b) $L_{e,I}$ against L, with fit to L_{KP}, compared to the ideal Kratky-Porod L_{KP} and rigid rod L. (c) $L_{e,N}$ of wormlike micelles with $L = 10$ μm, and L_O of a confined semiflexible polymer, against Π. (d) ΔL_e of wormlike micelles against fd virus L/P, compared to $\Delta L_e'$.

volume effects [20]. The average end-to-end length is defined as $L_{\mathrm{KP}} = \sqrt{4P'P}(L/2P)^{\nu}$, where P' is an effective persistence length. For an ideal Kratky-Porod chain $P' = P$ and $\nu = 0.5$. We calculate L_e in the isotropic phase ($L_{e,I}$) for a range of L values and fit L_{KP} to our results for the range of wormlike micelle parameters. We find $P' = 0.573P$, and $\nu = 0.529$, shown in Fig. 3(b), where we also compare our results to the ideal Kratky-Porod wormlike chain and to the rigid-rod length L. Clearly, for shorter micelles, $L_{e,I}$ approaches L, while for longer ones, $L_{e,I}$ approaches the ideal Kratky-Porod length.

In the nematic fd virus phase, we can consider the polymer using the Odijk confined wormlike chain model [15], where the host nematic acts as a confining cylinder. The average end-to-end length is defined as $L_O = L\langle\omega \cdot \mathbf{n}\rangle$, proportional to the average $\omega \cdot \mathbf{n}$ along the chain, where $\mathbf{n}$ is the nematic director. We find that our predicted L_e at the I-N phase transition ($L_{e,N}$) is significantly below L_O [Fig. 3(c)], from which we infer that the host nematic is neither dense nor ordered enough to fully confine the polymer. By altering the stiffness of the host fd virus such that it is denser (flexible fd virus) or more ordered (rigid) at the transition (see Ref. [8]), we may confine better the polymer causing it to stretch out more over the I-N transition. Figure 3(d) shows $\Delta L_e = L_{e,N} - L_{e,I}$ for micelles of $L = 10$ μm, using a range of P values for the fd virus. Here we see that ΔL_e is largest when using very flexible fd virus. ΔL_e then decreases as the fd virus becomes stiffer, reaching a minimum, then increasing again for the most rigid fd virus studied. This presents the opportunity to tune the stretching of the polymers by varying the stiffness of the host fd virus. We also compare ΔL_e to $\Delta L_e' = L_O - L_{\mathrm{KP}}$ [Fig. 3(d)], finding that this qualitatively matches our nonmonotonic results.

In conclusion, we have developed a model for binary mixtures of semiflexible rods and applied it to binary fd virus mixtures. The addition of flexibility in our model gives results that are quantitatively much closer to experimental data than those obtained using rigid rods [6]. The key reason appears to lie in the effective shape of the rods, which changes throughout the phase diagrams and can effectively render them a mixture of rods of differing diameter and length, indicating that any static-shaped rigid-rod model will miss some of the essential physics. In addition, we have studied the stretching of semiflexible polymers in an fd virus solvent. We find that sufficiently short polymers stretch out considerably over the I-N transition of the host solvent, while for the longer ones some stretching is observed, but the effect is much less pronounced. Changing the stiffness of the host fd virus can greatly increase the stretching effect. We hope that our findings will stimulate further experimental explorations, and believe that extensions of the theory to, e.g., inhomogeneous states and nonequilibrium phenomena are within reach of the present model.

Financial support of a FOM and a NWO-VICI grant is acknowledged.

[1] S. Chandrasekhar, *Liquid Crystals* (Cambridge University Press, Cambridge, England, 1993), 2nd ed.
[2] G. J. Vroege and H. N. W. Lekkerkerker, Rep. Prog. Phys. **55**, 1241 (1992).
[3] J. Tang and S. Fraden, Liq. Cryst. **19**, 459 (1995).
[4] Z. Dogic and S. Fraden, Phil. Trans. R. Soc. A **359**, 997 (2001).
[5] E. Grelet, Phys. Rev. Lett. **100**, 168301 (2008).
[6] K. R. Purdy, S. Varga, A. Galindo, G. Jackson, and S. Fraden, Phys. Rev. Lett. **94**, 057801 (2005).
[7] R. van Roij, B. Mulder, and M. Dijkstra, Physica (Amsterdam) **261A**, 374 (1998).
[8] See supplemental material at http://link.aps.org/supplemental/10.1103/PhysRevLett.106.208302 for a complete outline of the method presented here.
[9] H. Fynewever and A. Yethiraj, J. Chem. Phys. **108**, 1636 (1998).
[10] A. N. Semenov and A. V. Subbotin, Polym. Sci. USSR **31**, 2266 (1989).
[11] Z. Dogic *et al.*, Phys. Rev. Lett. **92**, 125503 (2004).
[12] A. R. Khokhlov and A. N. Semenov, Physica (Amsterdam) **108A**, 546 (1981); **112A**, 605 (1982).
[13] Z. Y. Chen, Macromolecules **26**, 3419 (1993).
[14] M. Dijkstra and D. Frenkel, Phys. Rev. E **51**, 5891 (1995).
[15] T. Odijk, Macromolecules **19**, 2313 (1986).
[16] P. P. F. Wessels and B. M. Mulder, Soft Mater. **1**, 313 (2003); J. Phys. Condens. Matter **18**, 9335 (2006).
[17] G. J. Vroege and H. N. W. Lekkerkerker, J. Phys. Chem. **97**, 3601 (1993).
[18] E. Barry, D. Beller, and Z. Dogic, Soft Matter **5**, 2563 (2009).
[19] O. Kratky and G. Porod, J. Colloid Sci. **4**, 35 (1949).
[20] H.-P. Hsu, W. Paul, and K. Binder, Macromolecules **43**, 3094 (2010).